Available online at www.sciencedirect.com
ScienceDirect
Journal of the European Ceramic Society 28 (2008) 2039–2047
www.elsevier.com/locate/jeurceramsoc

Analyzing indentation behavior of $LaGaO_3$ single crystals using sharp indenters

Siddhartha Pathak [a,*], Surya R. Kalidindi [a], Benedikt Moser [b], Christine Klemenz [c], Nina Orlovskaya [d]

[a] *Department of Materials Science and Engineering, Drexel University, 3141 Chestnut Street, LeBow 344, Philadelphia, PA 19104, USA*
[b] *Materials Technology Section, EMPA Materials Science and Technology, 3602 Thun, Switzerland*
[c] *Advanced Materials Processing and Analysis Center, University of Central Florida, Orlando, FL 32816, USA*
[d] *Department of Mechanical, Materials, and Aerospace Engineering, University of Central Florida, Orlando, FL 32816, USA*

Received 5 September 2007; received in revised form 22 January 2008; accepted 8 February 2008
Available online 1 April 2008

Abstract

In this work, the mechanical properties of (1 0 0) and (0 0 1) oriented $LaGaO_3$ single crystals have been studied using sharp indenters. Vickers hardness values for both the (1 0 0) and (0 0 1) samples were found to be in the same range (~8 GPa). The values for the indentation fracture toughness (K_R) from Vickers indentation on the (1 0 0) samples were determined to be 0.8 ± 0.2 MPa m$^{1/2}$. Different crack lengths, implying a strong anisotropy in the indentation fracture toughness values, were observed in the two mutually perpendicular directions in the indentations on the (0 0 1) samples. These measurements led to estimates of 0.5 ± 0.1 and 1.3 ± 0.3 MPa m$^{1/2}$ for the two different sets of cracks on the (0 0 1) samples. In situ nanoindentation inside the SEM using a cube-corner indenter has also been used for studying the indentation fracture response of these samples.
© 2008 Elsevier Ltd. All rights reserved.

Keywords: Perovskites; Hardness; Mechanical properties; Toughness; Indentation; $LaGaO_3$

1. Introduction

Lanthanum gallate-based ceramics are good candidates for substrate material for high temperature superconductors (HTSCs)[1] and colossal magnetoresistive film epitaxy.[2] They are also considered to be attractive alternatives to cubic zirconia for use as electrolytes in intermediate temperature (650–800 °C) solid oxide fuel cells (IT-SOFCs). Lanthanum gallate is a pure ionic conductor over a wide range of oxygen partial pressures and exhibits high oxygen conductivity at 700 °C, comparable to zirconia at 1000 °C.[3,4]

The mechanical properties of the gallates are critical for long-term operation of multilayered electrical devices containing these materials. The application of these materials in high temperature electrochemical cells demands sufficient mechanical strength and high creep resistance. Very few reports have focused on these problems associated with the reliability of the SOFC materials. Vasylechko et al.[5] have noted that most of the properties (such as thermal expansion) have been measured on polycrystalline $LaGaO_3$-based ceramic samples which yield only average properties. Investigation of single crystal samples could assess anisotropy of the physical properties in different crystallographic directions.

Baskaran et al.[6] have noted that fracture toughness obtained by the indentation method is typically less than fracture toughness measured by other macroscopic techniques such as the notched beam method. However, the indentation fracture toughness is quite useful in quickly evaluating various candidate materials and ranking them on a relative scale. The indentation toughness of polycrystalline LSGM compositions was reported to be in the range of 0.9–1.1 MPa m$^{1/2}$, while the hardness measured by indentation with a Vickers diamond pyramid was 7.0–8.2 GPa.[6,7] Giess et al.[8] reported the indentation fracture toughness and Vickers hardness (H) values for single crystal $LaGaO_3$ as 0.7 MPa m$^{1/2}$ and 9.4 GPa, respectively. The authors also noted that the cracks tend to follow the cleavage planes in

* Corresponding author. Tel.: +1 267 243 9492; fax: +1 215 895 6760.
E-mail address: sp324@drexel.edu (S. Pathak).

0955-2219/$ – see front matter © 2008 Elsevier Ltd. All rights reserved.
doi:10.1016/j.jeurceramsoc.2008.02.010

the crystal, and oriented the indentations as to yield cracks propagating collinearly with the contact impression diagonals. The indentation fracture toughness for the polycrystalline LSGM-1020 (0.9–1.1 MPa $m^{1/2}$)[6] is slightly higher than that of the single crystal $LaGaO_3$ (0.7 MPa $m^{1/2}$)[6,8] which is indicative of the increased resistance to crack penetration in a polycrystalline assemblage. The indentation fracture toughness of all the lanthanum gallates have been found to be significantly lower than the corresponding values for polycrystalline cubic zirconia electrolyte materials (2–3 MPa $m^{1/2}$).[6,9]

The anisotropy of the coefficient of thermal expansion of $LaGaO_3$ single crystals was reported in Ref. 5. The anisotropy in the mechanical properties of these single crystals is largely unknown. In this paper, we investigated the difference in mechanical properties of $LaGaO_3$ single crystals grown in the [0 0 1] and [1 0 0] directions using indentation techniques. It is reiterated here that the literature reports described earlier focused mostly on mechanical properties measured only along selected growth directions of $LaGaO_3$. To the best of our knowledge, this is the first time that a detailed study on anisotropy of the mechanical properties of single crystalline $LaGaO_3$ substrates grown in different directions is reported. This report deals with indentation by sharp indenters, namely Vickers and cube-corner indenter. In this article, hardness and indentation fracture toughness by Vickers microindentation are presented along with in situ nanoindentation with a cube-corner indenter inside the SEM providing new insights into the deformation mechanisms of $LaGaO_3$ single crystals.

2. Crystal structure

$LaGaO_3$ belongs to the space group $D_{2h}{}^{16}$-*Pbnm* of the orthorhombic system having four formula units, $Z=4$, with $a=5.52299$ Å, $b=5.49138$ Å, $c=7.7725$ Å[10,11] at ambient temperature. Heating of the orthorhombic (o) $LaGaO_3$ to 143.5 °C leads to a first-order phase transition to $R\bar{3}c$ rhombohedral (r) phase with cell parameters being $a=3.889$ Å, $\alpha=89.50°$.[12] Some authors[13] have suggested a considerable higher temperature (875 °C) for the phase transition, but recent studies[1,14] are in agreement with the lower transition temperature. A second-order phase transition from rhombohedral to monoclinic structure has also been suggested[15] in the temperature range ~750 to ~1000 °C. The melting point of $LaGaO_3$ is 1800 °C.[12]

The appearance of twins is common in the perovskite and related structures. It should be noted that although the coefficient of thermal expansion (CTE) for $LaGaO_3$ above the transition temperature provides an ideal lattice match for high temperature superconducting films, the presence of the disruptive low-temperature phase transition and a strong tendency for twinning restrict its wider application as a substrate material.[8,10] Two views exist on the possible reason for the formation of these twins in $LaGaO_3$. According to some authors,[5,16] the $LaGaO_3$ crystals are heavily twinned in order to accommodate the strain originating from the first-order phase transition. Others, however[17,18] have suggested that the formation of twins in $LaGaO_3$ crystals grown by the Czochralski method occurs at temperatures above 500 °C and is caused by the thermoelastic stresses occurring when the crystal is pulled.

Transformation twins in $LaGaO_3$ were studied in detail in Ref. 16. They are related by a point symmetry element lost during phase transition to a lower point group. The lost element might be a mirror plane, a rotation axis or an inversion center. The twins represent the orientation variants associated with a reduction in point group symmetry. The $\{1\,0\,1\}_o$, $\{1\,2\,1\}_o$ and $\{1\,1\,0\}_r$ twins were observed in $LaGaO_3$ single crystals cycled through o → r transition temperature using optical microscopy,[12,19] TEM[16] and synchrotron X-ray tomography.[12,20] From the space group symmetry only the reflection and rotation twins may occur upon the o → r phase transition since both $LaGaO_3$ phases are centrosymmetric.[16,21]

3. Processing of single crystals

For this research, single crystals of $LaGaO_3$ were grown by conventional RF-heating Czochralski technique with automatic diameter control.[22] The starting chemicals, La_2O_3 and Ga_2O_3 of 99.99% and 99.999% purity, respectively, were dried and mixed in the stoichiometric 1:1 ratio and hydrostatically pressed into tablets. The charge was then molten in an iridium crucible of 40 mm diameter and 40 mm height by using RF heating. Crystal pull rate was typically 3–4 mm/h, with a crystal rotation of 40 rpm. The growth atmosphere consisted of a mixture of 98% nitrogen with 2% oxygen to prevent gallium oxide evaporation during growth. Crystals up to 2.5 cm diameter and 10 cm length were grown in the [1 0 0] and [0 0 1] directions. The crystals were oriented by X-ray Laue back-reflection method, and were cut into (1 0 0) and (0 0 1) in-plane oriented square wafers of 1 mm thickness. The wafers were then polished by standard techniques. The optical micrographs of the (1 0 0) and (0 0 1) $LaGaO_3$ crystals along with a schematic representation of the single crystal growth and direction of indentation are shown in Fig. 1.

Twin density in a given crystal/wafer depends on growth process parameters, particularly on the quality and orientation of the seed used for the growth. By applying pressure along certain crystallographic directions while heating through the phase transition temperature, the twin-boundaries in $LaGaO_3$ can be moved and single-domain crystals can be obtained. A detwinning procedure similar to that described in Ref. 23 was applied to the [0 0 1] crystal investigated in this study. In this detwinning procedure, the substrate is heated above the phase transition temperature under a pressure of about 6–12 MPa applied in the [0 0 1] direction. The substrate is then cooled to room temperature under the same pressure. This enables to move majority of twins out of the substrates. The detwinning procedure is only successful when performed on high-quality substrates. Indeed, the substrates used for detwinning procedure are cut from bulk crystal regions that already show a low density of twins.

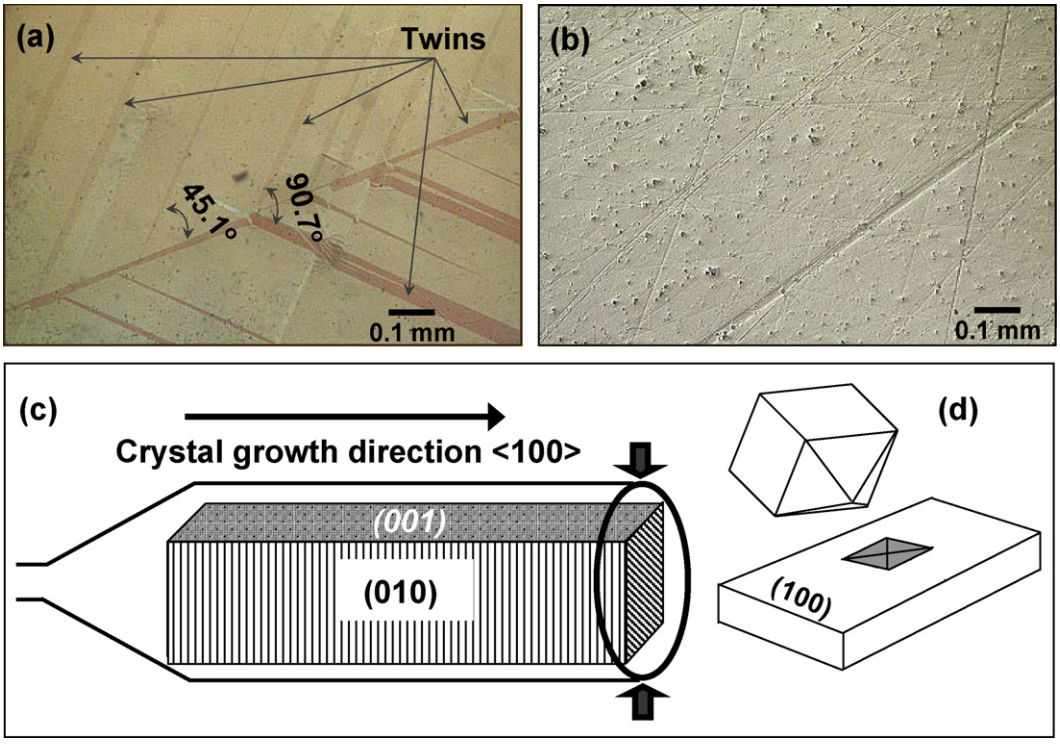

Fig. 1. Nomarski differential interference contrast (NDIC) microphotograph of (a) the twin structure in the (1 0 0) $LaGaO_3$ single crystal and (b) the surface of a (0 0 1) $LaGaO_3$ single crystalline substrate. The surface defects seen in (b) are probably artifacts generated during polishing/grinding of these crystals. Schematic representation (c) of the growth direction and preparation of the bulk Czochralski-grown $LaGaO_3$ crystal, and (d) of the Vickers indentation. The indentation direction is perpendicular to the (1 0 0) plane. Similar indentation was performed on (0 0 1)-cut substrates.

4. Experimental details

4.1. Vickers hardness and fracture toughness by microindentation

Micro-hardness tests were performed using a Vickers micro-hardness tester (LECO M-400). A Vickers diamond indenter in the form of a pyramid with a square base and an angle of 136° between opposite faces was used for the test. The sample was subjected to loads of 0.49, 0.98, 1.96, 2.94, 4.9 and 9.8 N for a period of 10 s. The Vickers hardness H (GPa) was calculated according to the following formula[24]:

$$H\,(\mathrm{GPa}) = 0.018187\frac{P}{d^2} \tag{1}$$

where P is the load in N, and d is the arithmetic mean of the two diagonals in m.

The indentation fracture toughness K_R was calculated from the resulting Vickers indentation by using the following formula[25]:

$$K_R\,(\mathrm{MPa}\sqrt{m}) = \chi\left(\frac{E}{H}\right)^{1/2}\frac{P}{a^{3/2}} \tag{2}$$

where P is the applied load in N, E is the Young's modulus in GPa, H is the Vickers hardness in GPa, a is the corner crack length measured from the center of the indent in m, and χ is an empirically determined "calibration" constant taken to be 0.022 in ambient air.[26,27] The modulus values used to calculate K_R were obtained from spherical nanoindentation experiments described in the companion paper.[28] Two samples of each orientation ($LaGaO_3$ (1 0 0) and (0 0 1)) were chosen for the tests. The average of five tests at each load was used for reporting the hardness and fracture toughness values.

4.2. In situ nanoindentation inside the SEM

Nanoindentation is widely used to measure the hardness and Young's modulus of a material.[29,30] Some recent studies have also used the technique to measure indentation fracture toughness of different materials.[26,31] In a typical nanoindentation test, the load–displacement data is measured continuously during the test. Other information, such as the size and geometry of the impression after test and the distribution and size of cracks that may be generated during test, is assessed after the indentation. Insights into the material behavior may be obtained by post-mortem investigations of the indentation area and/or relating the indentation characteristics to theoretical simulations. In many cases, however, such correlations are not easy. For example, it may not be clear whether the cracks, visible after the indentation, formed during loading or unloading. Crack lengths can be difficult to measure as cracks are often closed after unloading and are therefore almost impossible to visualize. The real contact area may be overestimated as a result of such crack formation leading to inaccurate hardness values. Also material pile-up during nanoindentation is not revealed in the load–displacement data but can significantly affect the hardness

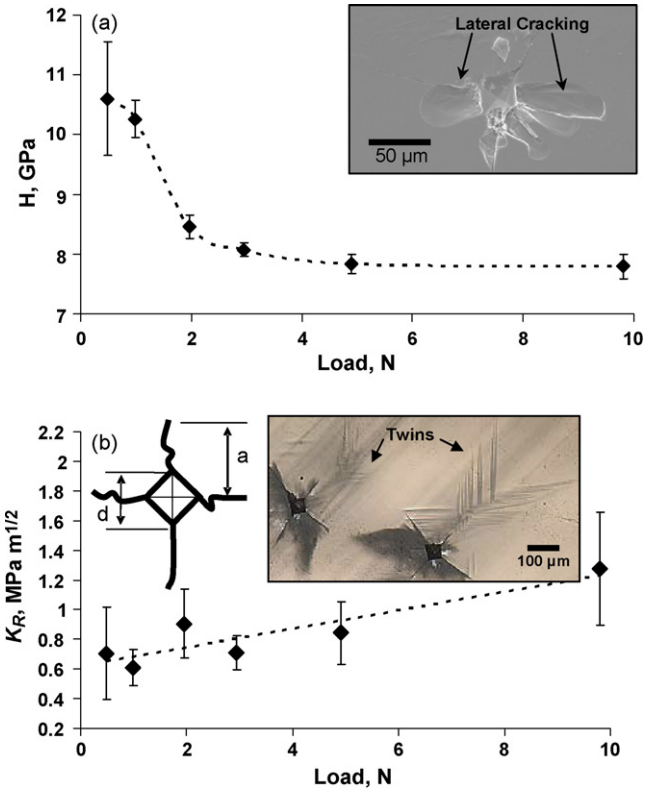

Fig. 2. Microindentation of the (1 0 0) $LaGaO_3$ single crystal. (a) Vickers hardness. Inset: SEM image of Vickers impression (9.6 N load) with significant lateral cracking. (b) Vickers fracture toughness. Insets: A schematic of K_R measurement using Vickers impression and crack measurements. Twins generated on the (1 0 0) crystal due to Vickers indentation.

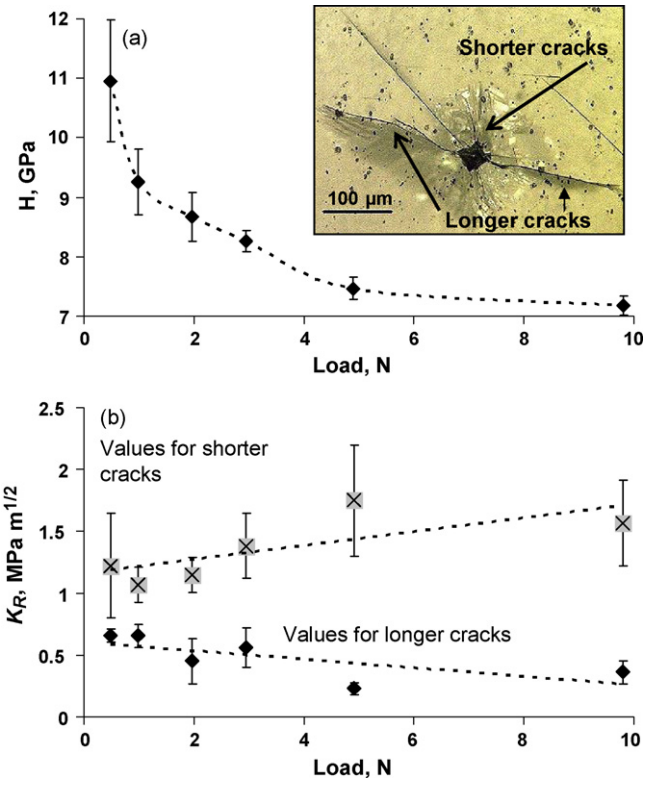

Fig. 3. Microindentation of the (0 0 1) $LaGaO_3$ single crystal. (a) Vickers hardness. Inset: optical micrograph of Vickers impression (9.6 N load) taken with Nomarski contrast prism showing the longer cracks in one direction and shorter cracks in the direction perpendicular to it. (b) Vickers fracture toughness measured separately for two perpendicular directions.

value. These and many other such difficulties have been outlined in Ref. 32. In situ nanoindentation tests inside the SEM chamber have the advantage of observing the surface around the tip during the loading/unloading cycle and therefore provide additional information about material pile-up, sinking-in or the onset and propagation of cracks under load.

In situ indentation experiments were performed using a custom-built instrumented in situ indenter inside a Zeiss DSM 962 SEM chamber. The instrument has been described in detail elsewhere.[32] The indenter assembly consists of an x–y stage for sample positioning and scratching, while indentation is performed along the z-axis. The indentation axis is inclined by about 70° with respect to the electron beam. This allows continuous observation of the area around the indent during the loading/unloading cycle, simultaneously with the acquisition of the load and displacement values.[33]

All measurements for the in situ nanoindentation have been done using a diamond cube-corner indentation tip. The smaller effective cone angle (the angle of the cone that provides the same area to depth relationship as the actual indenter) of the cube-corner geometry (42.28°) compared to the commonly used Vickers (70.3°), Berkovich (70.3°) or spherical tips guarantees a better view of the indentation zone with the SEM. However it should be noted here that due to the different indenter geometry, the load–displacement curves measured with cube-corner tips have different shapes compared to curves measured with other tip geometries such as spherical.

In situ indentation measurements were performed in load-control mode to loads of 100 and 150 mN. The samples were coated with a conductive ∼2-nm thick coating for use inside the SEM. The SEM observations were recorded as a video file at a rate of 4.6, 6.9 and 3.5 s per frame (for Figs. 4–6, respectively) and later synchronized with the load–displacement curve to provide a one-to-one correlation between each video frame and its corresponding position on the load–displacement curve. It is to be noted that at most only 2/3rd of the events can be seen in the video (1/3rd is happening behind the 3-sided pyramid). Additionally, in order to get a high resolution video output, the observed region is sometimes further reduced to only around 1/3rd.

5. Results and discussion

5.1. Vickers hardness and fracture toughness by microindentation

$LaGaO_3$ is a relatively soft material (H is around 8 GPa). As seen from Figs. 2a and 3a, the H values decrease with increasing loads up to asymptotic values of ≈8 ± 0.4 and ≈7 ± 0.3 GPa (Eq. (1)) for (1 0 0) and (0 0 1) $LaGaO_3$ single crystals (the indentation direction was perpendicular to the (1 0 0) and (0 0 1) planes), respectively. The standard deviation is significantly reduced at increasing loads. Such decrease in hardness with increase in load has been reported for different materials and can be explained

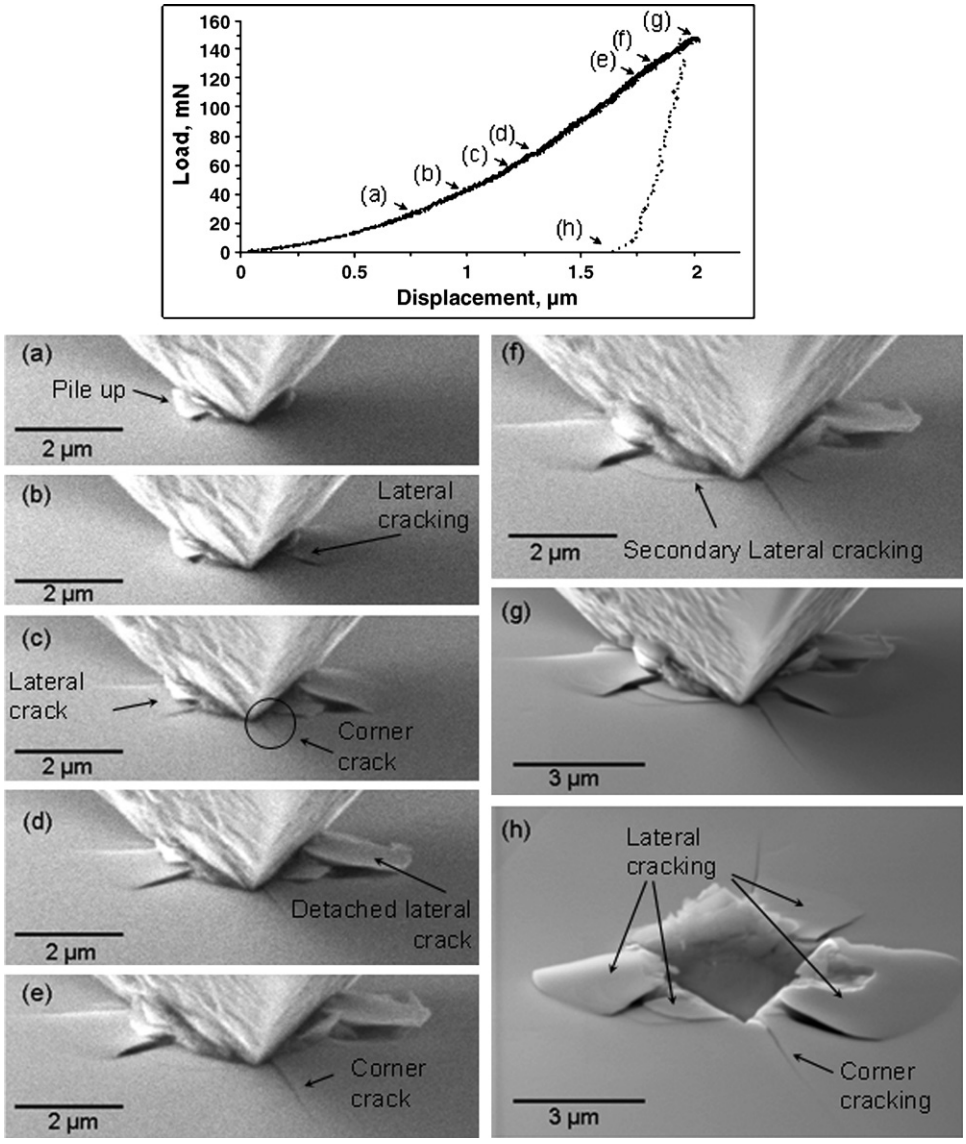

Fig. 4. SEM indentation made on (1 0 0) $LaGaO_3$ single crystal. The indentation process was recorded as a video file from which individual picture frames were extracted corresponding to a particular event during the loading/unloading cycle (indicated by arrows on the load–displacement graphs). Note the lower magnification in (g) and (h).

by the indentation size effect[34–36] or appearance of microcracks above a certain load that leads to a decrease in hardness.[37]

The indentation fracture toughness of (1 0 0) $LaGaO_3$ single crystal was found to increase with load from 0.7 MPa $m^{1/2}$ at 0.49 N load to 1.3 MPa $m^{1/2}$ at 9.8 N. It is possible this apparent increase in K_R is a consequence of the use of Eq. (2).[25] Another possible explanation for this is that it is a consequence of the deformation twinning that was often observed at the tip of the corner cracks in the (1 0 0) crystal (Fig. 2b inset). It was noted that higher applied loads produced more deformation twins. Deformation twins are known to increase strain hardening rates and ductility of metals.[38,39] In addition to the corner cracks (cracks originating from the corners of the Vickers indentation) that was used for K_R calculations, significant lateral cracking (cracks from the lateral edges) has also been observed during indentation especially at higher loads, as one can see from the inset of the optical micrograph of the twinning (Fig. 2a inset).

However, for the (0 0 1) $LaGaO_3$ single crystal the crack lengths were significantly larger in one direction compared to the perpendicular direction. These directions remained unchanged, even when the sample was rotated with respect to the indenter before the indentation. The fracture toughness values were calculated as being ≈0.5 MPa $m^{1/2}$ for the longer cracks and ≈1.3 MPa $m^{1/2}$ for the shorter ones (Fig. 3b) indicating that these two perpendicular directions in the plane of the sample are different with respect to their toughness. The dependence of K_R values on the applied load was less for the (0 0 1) samples than the (1 0 0) samples which correlated well with the absence of twins in the (0 0 1) single crystal.

5.2. *In situ nanoindentation inside the SEM*

Load–displacement curves measured inside the SEM on the (1 0 0) and (0 0 1) $LaGaO_3$ single crystals are shown in Figs. 4–6.

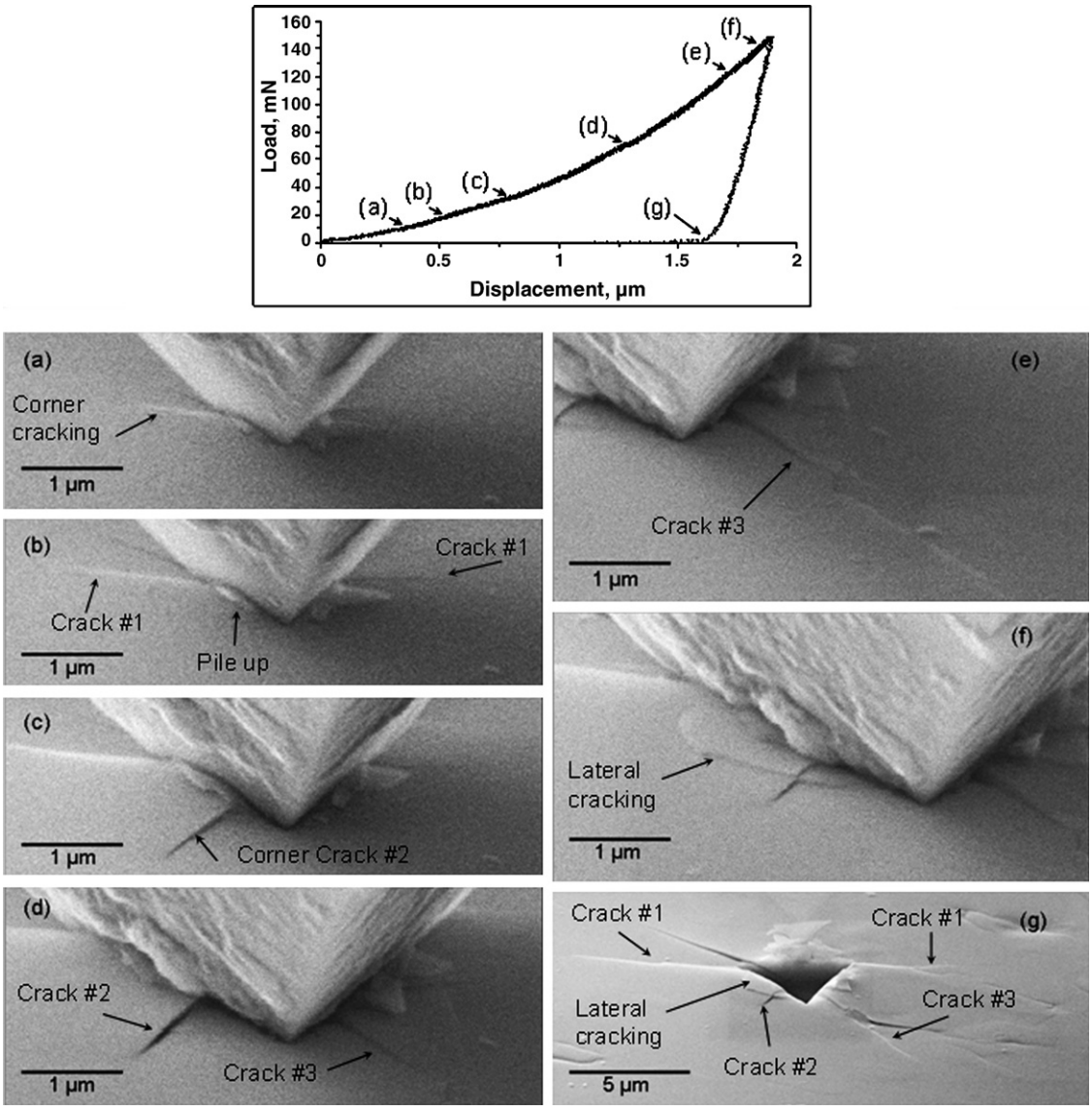

Fig. 5. SEM indentation made on (0 0 1) $LaGaO_3$ single crystal. The indentation process was recorded as a video file from which individual picture frames were extracted corresponding to a particular event during the loading/unloading cycle (indicated by arrows on the load–displacement graphs). Cracks #1, #2 and #3 are corner cracks originating at different loads under the indenter. Note the lower magnification in (g).

For all samples, individual picture frames were extracted from the indentation video file corresponding to a particular event during the loading/unloading cycle indicated by arrows on the load–displacement graphs.

Within the accuracy of the instrument, the load–displacement curve for (1 0 0) $LaGaO_3$ single crystal (Fig. 4) is smooth and does not indicate any significant pop-in (during loading) or pop-out (during unloading) events that can be correlated to crack formation or phase transformation. However the SEM video images suggest otherwise. The SEM images reveal that at 25 mN applied load a clear pile-up around the indentation tip is visible (Fig. 4a) that cannot be inferred from the load–displacement data. With increasing load, this pile-up becomes more pronounced and lateral cracks start growing and become visible (Fig. 4b and c). As the load continues to increase to around 60 mN, initiation of corner cracking can be observed (Fig. 4c, the crack is marked by a circle). At a load of around 70 mN a small discontinuity in the load–displacement curve is visible which corresponds to the moment when the upper right part of the lateral crack (Fig. 4d) becomes completely detached from the specimen. Further increase in load does not show any other major event other than the continuous growth of the corner crack (Fig. 4e and f), with small secondary lateral cracks being developed at about 140 mN (Fig. 4f). The indenter was stopped at a maximum load of 150 mN (Fig. 4g). The residual impression after the indenter was removed (Fig. 4h) shows the extensive lateral cracking and pile-ups. Similar lateral and corner cracking is also visible in Fig. 2a and b (insets) after Vickers indentation of the (1 0 0) $LaGaO_3$ single crystal. While a simple study of the residual impression by SEM cannot reveal the full details of the indentation process in general and the exact moment of crack initiation and occurrence of pile-up in particular, the in situ SEM techniques can be very useful in observing such details under contact loading. Note that, as in the case of Vickers indenta-

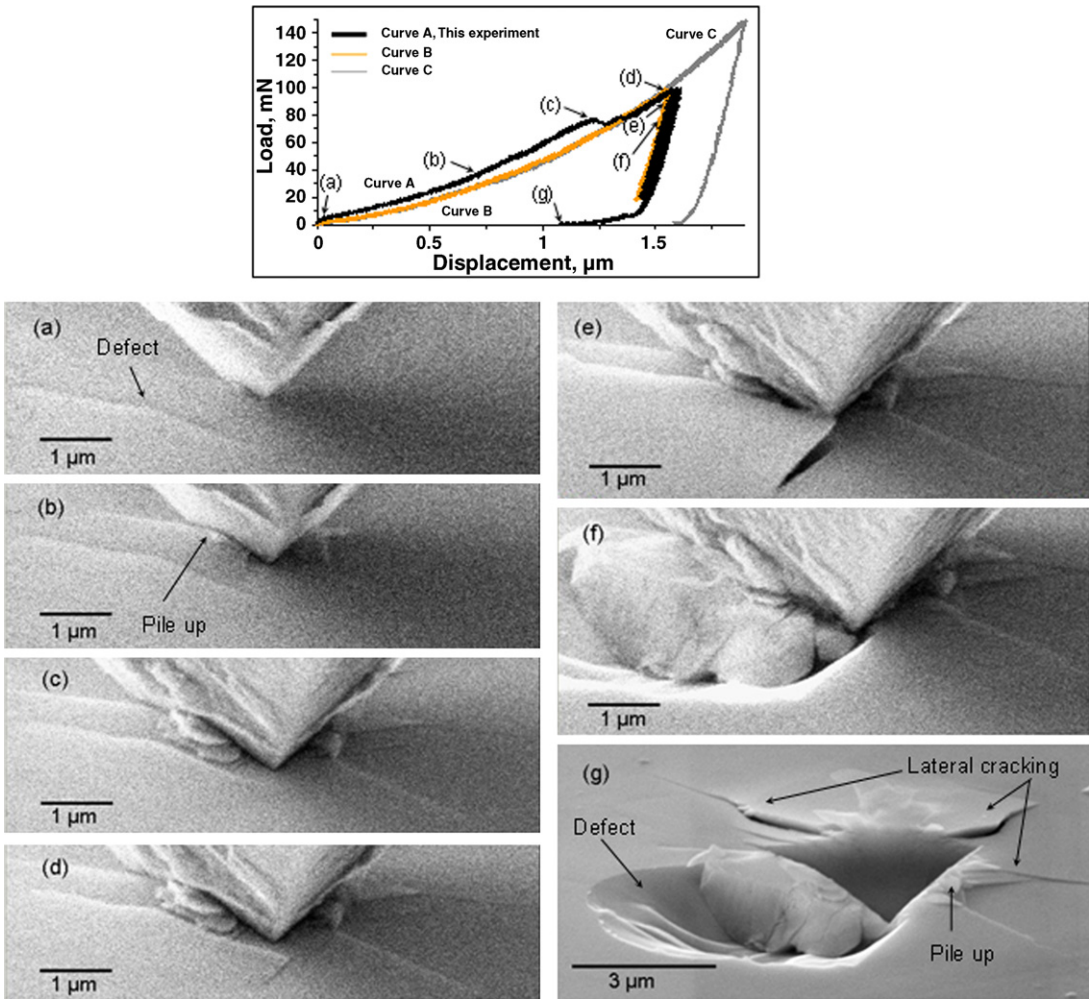

Fig. 6. SEM indentation made on (0 0 1) $LaGaO_3$ single crystal. The indentation process was recorded as a video file from which individual picture frames were extracted corresponding to a particular event during the loading/unloading cycle (indicated by arrows on the load–displacement graphs). A prominent pop-in can be seen at a point 'c' in the curve at around 75 mN. After the pop-in event the curves converge back together. The curve A is the load–displacement curve for this particular experiment. The curves B and C, which are similar curves at the same and higher maximum loads respectively, on different locations of the same sample, are used for comparison. Note the lower magnification in (g).

tion, there was no significant difference in the size of the cracks formed on the three edges of the cube-corner indenter for the (1 0 0) $LaGaO_3$ single crystal.

The load–unload curve for the (0 0 1) $LaGaO_3$ single crystal sample presented in Fig. 5 is comparable to the one measured for the (1 0 0) sample. At the same time, the SEM images recorded during the nanoindentation cycle reveal a different behavior. Unlike the (1 0 0) sample, no lateral cracking was observed up to a significant load of 140 mN (Fig. 5f). Instead, the cracking started with the formation of corner cracks (marked as crack #1) which were preferentially growing in one particular direction (Fig. 5a–c). Even at higher loads of 80, 125 and 140 mN (Fig. 5d–f, respectively), no corner cracking had originated from the corner of the indenter facing the observer while the crack (#1) had grown significantly from the two corners in the back. This is an indication of the difference of the toughness in the two perpendicular directions of the $LaGaO_3$ single crystal, when one direction is much weaker/softer than the other. This is again in correspondence with the microindentation result (Fig. 3a inset) where Vickers indentation shows the same behavior. It is worth mentioning here that unlike the indentation behavior of the (1 0 0) $LaGaO_3$ single crystal, the pile-up during the nanoindentation of (0 0 1) sample occurs after the corner cracks have already been formed (Fig. 5b). Two other corner cracks (cracks #2 and #3) are forming at a load of around 30 and 40 mN as seen in Fig. 5c and d, respectively. The micrograph of the residual impression after the nanoindentation (Fig. 5g) shows significant lateral cracking and pile-up. The corner crack (#1) can be seen to have significantly grown in one specific direction and appear to be relatively larger than cracks #2 and #3. This observation is in agreement with the results from Vickers indentation described earlier (Fig. 3), where two different cracks lengths were noted in two perpendicular directions. Lateral cracking has occurred after the indenter has been removed, and pile-up is also visible after the nanoindentation.

Repeated load–unload cycles (three times) were also performed for both (0 0 1) and (1 0 0) $LaGaO_3$ single crystals at different loads. The experiments did not reveal any significant

changes occurring after the first load–unload cycle as observed from the video and SEM images. There was no hysteresis observed in the reload–unload cycles. As in the case of the Vickers indents, the direction of the longer cracks in the (0 0 1) sample was unchanged even when the sample was rotated with respect to the indenter before the indentation.

Compared to the smooth load–displacement curves obtained in Figs. 4 and 5 the loading part of the (0 0 1) $LaGaO_3$ single crystal in Fig. 6 (curve A) shows a prominent pop-in event, i.e. sudden increases of the displacement at constant load. The origin of this pop-in event can be explained by the presence of a large defect next to the indentation site which results in pull-out of a lateral crack chip. The subsurface defect is visible before the indentation (Fig. 6a), and its presence is also revealed during the nanoindentation process. The initial part of the loading curve (curve A) shows a small change in slope at around 5 mN (point a ~0.06 μm in the load–displacement curve). The corresponding SEM image (Fig. 6a) does not show any significant event occurring at that load. One possible explanation for this change of slope could be that the indenter 'felt' the presence of the defect at this point. This is also suggested by the deviation of the loading curve A from the point 'a' onwards when compared to other similar curves (curves B and C) on the same sample but at different locations and at different load levels. After the pop-in has occurred at around 75 mN all the curves converge back together. The SEM images recorded after this initial change in slope (Fig. 6b–e) show the formation and growth of corner cracks in a preferential direction similar to the previous indentation shown in Fig. 5. The huge pop-in the loading curve occurred at a load of about 75 mN (Fig. 6c). This is indicative of the defect forming or cracks propagating in the sample due to nanoindentation. As nothing significant is visible on the surface of the crystal during loading (Fig. 6c and d) cracks are probably forming below the surface or behind the indenter. It is only during the unloading of the indenter (Fig. 6e and f) when a large lateral crack chip is generated with a resulting depression. It is also worth mentioning here that no hysteresis has been observed following repeated load–unload cycles at the same location. The residual impression after the removal of the indenter shows the presence of the large depression as well as significant lateral cracking occurring behind the indenter tip (Fig. 6g). The above evidence shows that only such severe sample modifications, like pull-out of a lateral crack chip, can be seen distinctly in the load–displacement curve. This has been previously reported in Ref. 32 where a discontinuity in the load–displacement curve was related to the delamination of a large part of the coating material on the sample.

6. Conclusions

Mechanical properties and in situ nanoindentation inside the SEM of (1 0 0) and (0 0 1) $LaGaO_3$ single crystals are reported in this article. Hardness and fracture toughness have been measured by Vickers microindentation. While reported hardness values are very similar for the $LaGaO_3$ single crystals grown in different crystallographic directions, the indentation crack propagation behavior is very different. Lateral cracks have been found to develop during the indentation of the (1 0 0) $LaGaO_3$ single crystal, and deformation twins have also been observed at the tip of the moving crack during indentation leading to the formation of shorter Vickers cracks. For the (0 0 1) single crystal the length of cracks originating from the corner of the Vickers impression in one direction is significantly larger than in the perpendicular direction. The in situ nanoindentation with a cube-corner tip revealed the different stages of the indentation process visible on the crystal surface such as pile-up, corner and lateral cracking. The sequence of these events are different in the two different single crystals; lateral cracking occurs significantly later in the (0 0 1) $LaGaO_3$ single crystal compared to the (1 0 0) crystal. These events do not lead to significantly distinct features on the indentation load–displacement curves, and only major events such as defect pull-outs can be correlated to pop-ins in the nanoindentation curve.

Acknowledgement

This work was supported by the National Science Foundation through grant number DMR-0201770.

References

1. Sandstrom, R. L., Giess, E. A., Gallagher, W. J., Segmüller, A., Cooper, E. I., Chisholm, M. F. *et al.*, Lanthanum gallate substrates for epitaxial high-temperature superconducting thin films. *Applied Physics Letters*, 1988, **53**(19), 1874–1876.
2. Kawasaki, M., Izumia, M., Konishia, Y., Manakoa, T. and Tokuraa, Y., Perfect epitaxy of perovskite manganite for oxide spin-electronics. *Materials Science and Engineering B*, 1999, **63**(1–2), 49–57.
3. Feng, M. and Goodenough, J. B., A superior oxide-ion electrolyte. *European Journal of Solid State and Inorganic Chemistry*, 1994, **31**(8–9), 663.
4. Ishihara, T., Matsuda, H. and Takita, Y., Doped $LaGaO_3$ perovskite type oxide as a new oxide ionic conductor. *Journal of the American Chemical Society*, 1994, **116**(9), 3801–3803.
5. Vasylechko, L., Vashookc, V., Savytskiia, D., Senyshyna, A., Niewab, R., Knappd, M. *et al.*, Crystal structure, thermal expansion and conductivity of anisotropic $La_{1-x}Sr_xGa_{1-2x}Mg_{2x}O_{3-y}$ ($x = 0.05$, 0.1) single crystals. *Journal of Solid State Chemistry*, 2003, **172**(2), 396–411.
6. Baskaran, S., Lewinsohn, C. A., Chou, Y.-S., Qian, M., Stevenson, J. W. and Armstrong, T. R., Mechanical properties of alkaline earth-doped lanthanum gallate. *Journal of Materials Science*, 1999, **34**, 3913–3922.
7. Stevenson, J. W., Armstrong, T. R., Pederson, L. R., Li, J., Lewinsohn, C. A. and Baskaran, S., Effect of A-site cation nonstoichiometry on the properties of doped lanthanum gallate. *Solid State Ionics*, 1998, **113–115**, 571–583.
8. Giess, E. A., Sandstorm, R. L., Gallagher, W. J., Gupta, A., Shinde, S. L., Cook, R. F. *et al.*, Lanthanide gallate perovskite-type substrates for epitaxial high-T_c superconducting $Ba_2YCu_3O_{7-\delta}$ films. *IBM Journal of Research and Development*, 1990, **34**(6), 916–926.
9. Lange, F. F., Transformation toughening. *Journal of Materials Science*, 1982, **17**, 240–246.
10. Vasylechko, L., Matkovski, A., Suchocki, A., Savytskii, D. and Syvorotka, I., Crystal structure of $LaGaO_3$ and $(La,Gd)GaO_3$ solid solutions. *Journal of Alloys and Compounds*, 1999, **286**, 213–218.
11. Lerch, M., Boysen, H. and Hansen, T., High-temperature neutron scattering investigation of pure and doped lanthanum gallate. *Journal of Physics and Chemistry of Solids*, 2001, **62**(3), 445–455.
12. Bdikin, I. K., Shmyt'ko, I. M., Balbashov, A. M. and Kazansky, A. V., Twinning of $LaGaO_3$ single crystals. *Journal of Applied Crystallography*, 1993, **26**, 71–76.

13. Geller, S., Crystallographic studies of perovskite-like compounds. IV. Rare earth scandates, vanadites, galliates, orthochromites. *Acta Crystallographica*, 1957, **10**, 243.
14. O'Bryan, H. M., Gallagher, P. K., Berkstresser, G. W. and Brandle, C. D., Thermal analysis of rare earth gallates and aluminates. *Journal of Materials Research*, 1990, **5**(1), 183.
15. Kobayashi, J., Tazoh, Y., Sasaura, M. and Miyazawa, S., Structural analysis of lanthanum gallate. *Journal of Materials Research*, 1991, **6**(1), 97–100.
16. Wang, W.-L. and Lu, H.-Y., Phase-transformation-induced twinning in orthorhombic $LaGaO_3$ $\{1\,2\,1\}$ and $[0\,1\,0]$ twins. *Journal of American Ceramic Society*, 2006, **89**(1), 281–291.
17. Morozov, A. N., Morozova, O. Y. and Ponomarev, N. M., Real Structure of single crystals of $LaGaO_3$ grown by the Czochralski method. I. X-ray diffraction and X-ray topographic methods. *Kristallografiya*, 1993, **38**, 149–159.
18. Morozova, O. Y., Morozov, A. N., Ponomarev, N. M., Stepareva, N. N., Kutsev, V. S. and Buzanov, O. A., Real Structure of single crystals of $LaGaO_3$ grown by the Czochrzlski method. III. High temperature investigation. *Kristallografiya*, 1993, **38**, 165–173.
19. Fink-Finowicki, J., Berkowski, M. and Pajaczkowska, A., Twinning structure of $LaGaO_3$ grown by the Czochralski method. *Journal of Materials Science*, 1992, **27**(1), 107–110.
20. Yao, G. D., Dudley, M., Wang, Y., Liu, X. and Liebermann, R. C., Synchrotron X-ray topography studies of twinning and the phase transition at 145 °C in $LaGaO_3$ single crystals. *Materials Science and Engineering A: Structural Materials: Properties, Microstructure and Processing A*, 1991, **132**(1–2), 23–30.
21. Bilby, B. A. and Crocker, A. G., The theory of the crystallography of deformation twinning. *Proceedings of the Royal Society of London. Series A, Mathematical and Physical Sciences*, 1965, **288**(1413), 240–255.
22. Hurle, D. T. J., The evolution and modelling of the Czochralski growth technique. *Journal of Crystal Growth*, 1987, **85**, 1–8.
23. Mazur, K., Fink-Finowicki, J., Berkowski, M. and Schell, N., Defects in detwinned $LaGaO_3$ substrates. *Acta Physica Polonica A*, 1997, **92**, 205–208.
24. Dieter, G. E., *Mechanical Metallurgy*. Mc-Graw-Hill Book Company, 2001.
25. Anstis, G. R., Chantikul, P., Lawn, B. R. and Marshall, D. B., A critical evaluation of indentation techniques for measuring fracture toughness. I. Direct crack measurements. *Journal of the American Ceramic Society*, 1981, **64**, 533–538.
26. Morris, D. J. and Cook, R. F., In situ cube-corner indentation of soda-lime glass and fused silica. *Journal of the American Ceramic Society*, 2004, **87**, 1494–1501.
27. Cook, R. F., *Strength Characterisation of Ceramics Using Controlled Indentation Flaws*. University of New South Wales, Sydney, NSW, Australia, 1985.
28. Pathak, S., Kalidindi, S. R., Klemenz, C. and Orlovskaya, N., Analyzing indentation stress–strain response of $LaGaO_3$ single crystals using spherical indenters. *Journal of the European Ceramic Society*, 2008, doi:10.1016/j.jeurceramsoc.2008.02.009.
29. Fischer-Cripps, A. C., A review of analysis methods for sub-micron indentation testing. *Vacuum*, 2000, **58**, 569–585.
30. Oliver, W. C. and Pharr, G. M., An improved technique for determining hardness and elastic modulus using load and displacement sensing indentation experiments. *Journal of Materials Research*, 1992, **7**(6), 1564–1580.
31. Morris, D. J., Vodnick, A. M. and Cook, R. F., Radial fracture during indentation by acute probes. II. Experimental observations of cube-corner and Vickers indentation. *International Journal of Fracture V*, 2005, **136**(1), 265–284.
32. Rabe, R., Breguet, J. M., Schwaller, P., Stauss, S., Haug, F. J., Patscheider, J. *et al.*, Observation of fracture and plastic deformation during indentation and scratching inside the scanning electron microscope. *Thin Solid Films*, 2004, **469–470**, 206–213.
33. Moser, B., Kuebler, J., Meinhard, H., Muster, W. and Michler, J., Observations of instabilites during plastic deformation by in-situ SEM indentation experiments. *Advanced Engineering Materials*, 2005, **7**(5), 388–392.
34. Ma, G. and Clarke, D. R., Size dependent hardness of silver single crystals. *Journal of Materials Research*, 1995, **10**(4), 853–863.
35. McElhaney, K. W., Vlassak, Y. Y. and Nix, W. D., Determination of indenter tip geometry and indentation contact area for depth-sensing indentation experiments. *Journal of Materials Research*, 1998, **13**, 1300–1306.
36. Nix, W. D. and Gao, H., Indentation size effects in crystalline materials: a law for strain gradient plasticity. *Journal of the Mechanics and Physics of Solids*, 1998, **46**(3), 411–425.
37. Quinn, G. D., Green, P. and Xu, K., Cracking and the indentation size effect for knoop hardness of glasses. *Journal of the American Ceramic Society*, 2003, **86**(3), 441–448.
38. Asgari, S., El-Danaf, E., Kalidindi, S. R. and Doherty, R. D., Strain hardening regimes and microstructural evolution during large strain compression of low stacking fault energy fcc alloys that form deformation twins. *Metallurgical and Materials Transactions A: Physical Metallurgy and Materials Science A*, 1997, **28**(9), 1781–1795.
39. Salem, A. A., Kalidindi, S. R. and Doherty, R. D., Strain hardening of titanium: role of deformation twinning. *Acta Materialia*, 2003, **51**(14), 4225–4237.